On the Nature and Behavior of Li Atoms in Si: A First Principles Study

Hyunwoo Kim,[†,||] **Kyoung Eun Kweon,**[‡,||] **Chia-Yun Chou,**[§] **John G. Ekerdt,**[†] **and Gyeong S. Hwang**[*,†,‡]

Department of Chemical Engineering, University of Texas at Austin, Austin, Texas 78712; Department of Electrical and Computer Engineering, University of Texas at Austin, Austin, Texas 78712; and Materials Science and Engineering Program, University of Texas at Austin, Austin, Texas 78712

On the basis of density functional theory calculations, we present the bonding and dynamic behavior of Li atoms in crystalline Si and how the incorporation of Li atoms affects the structure and stability of the host Si lattice. Our calculations clearly evidence that the inserted Li atom energetically prefers a tetrahedral interstitial site while exhibiting a shallow donor level. Because of their positive ionization, the interactions between neutral Li impurities are repulsive, suggesting that they favorably remain isolated, rather than clustered. We also find that the charge transferred from neutral Li is largely localized within the first nearest Si atoms, thereby effectively screening the positively ionized Li. In addition, our electronic structure analysis highlights that the charge transfer leads to a significant weakening of nearby Si—Si bonds by filling the antibonding sp^3 states of Si. The mobility of Li interstitials is also estimated in the neutral and positive charge states.

1. Introduction

Silicon-based materials have recently emerged as promising candidates for anodes in lithium-ion batteries because they exhibit a higher energy-storage capacity than the conventional graphite anode. Silicon (Si) has a theoretical lithium (Li) capacity of $Li_{4.4}Si \approx 4200$ mAh/g, which is more than $10\times$ greater than that of graphite (372 mAh/g).[1–3] Moreover, Si is safer, less expensive, and far more abundant than graphite. However, the practical use of Si as an anode material is hampered by its low intrinsic electrical conductivity and poor cycling performance.[4–7] In particular, the volume changes up to 400% during lithiation and delithiation can cause severe cracking and pulverization of the Si electrode and consequent capacity fading arising from the loss of electrical contacts. Considerable efforts have been made to overcome these problems, for instance, through structural modifications such as amorphous phases,[8–10] nanoparticles,[11,12] nanowires,[13] and alloying with active/inactive elements such as silicon—tin[14] and silicon—metal[15–18] composites. In addition, first principles calculations have recently been applied to investigate fundamental aspects of the structural changes and lithiation behavior of Si-based materials, yet many of which still remain unclear.

Recent studies[19–24] have provided evidence for the formation of various stable Li silicide crystalline phases such as $Li_{12}Si_7$, Li_7Si_3, $Li_{13}Si_4$, $Li_{15}Si_4$, and $Li_{22}Si_5$ during high-temperature lithiation. The Li-rich LiSi alloys no longer exhibit a continuous Si tetrahedral network; instead containing discrete Si fragments (Si_n, $n \leq 5$) depending on the Li/Si composition ratio. While the Si network can be easily disintegrated by lithiation, it has also been reported that the lithiated Si at room temperature tends to exhibit no crystalline phases,[25] possibly because of a kinetic barrier to crystallization. The kinetic effect can be more important at the onset of lithiation because the introduction of Li into a rather rigid Si network would be thermodynamically more unfavorable and thus the lithiated structure of Si would be more kinetically controlled, compared to a highly flexible Li-rich LiSi alloy. However, thus far, there has been no comprehensive study as to the dynamic behavior of Li in Si-based materials and also the influence of Li introduction on the stability of the host lattice, particularly in the early stages of lithiation.

In this work, we examine the structure, diffusion, and interaction of Li atoms in Si and how Li incorporation affects the nature of the Si bonding network using density functional theory calculations. We first present the atomic structure, stability and bonding mechanism of interstitial Li in crystalline Si (*c*-Si). The result also shows how Li introduction leads to weakening of nearby Si—Si bonds in *c*-Si. Next, Li diffusion rates and Li—Li interactions in the neutral and positive charge states are estimated. The calculation results provide some insight into the dynamic behavior of Li atoms and the effect of Li incorporation on destabilization of the Si lattice, particularly in the early stages of lithiation.

2. Computational Methods

The calculations reported herein were performed on the basis of density functional theory (DFT) within the generalized gradient approximation (GGA-PW91[26]), as implemented in the Vienna Ab-initio Simulation Package (VASP).[27–29] Spin polarization of the Li/Si system was also examined, but appears to be unimportant. The projector augmented wave (PAW) method with a planewave basis set was employed to describe the interaction between ion cores and valence electrons. The PAW method is, in principle, an all-electron frozen-core approach that considers exact valence wave functions. Valence configurations employed are as follows: $1s^2 2s^1$ for Li and $3s^2 3p^2$ for Si. An energy cutoff of 300 eV was applied for the planewave expansion of the electronic eigenfunctions. The Si host was modeled using a 216-atom supercell with a fixed lattice constant
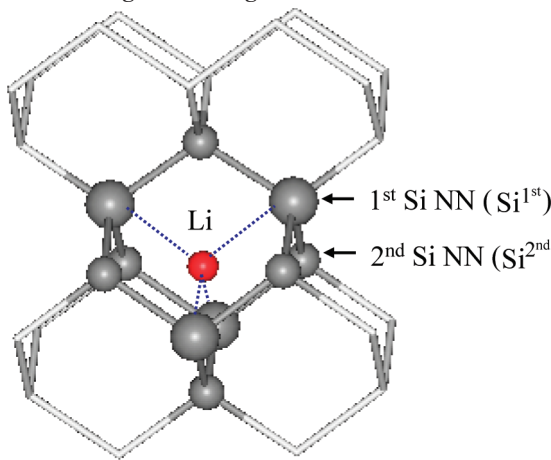
* To whom correspondence should be addressed: E-mail: gshwang@che.utexas.edu.
† Department of Chemical Engineering, University of Texas at Austin.
‡ Department of Electrical and Computer Engineering, University of Texas at Austin.
§ Materials Science and Engineering Program, University of Texas at Austin.
|| These authors contributed equally to this work.

Nature and Behavior of Li Atoms in Si

J. Phys. Chem. C, Vol. 114, No. 41, 2010 **17943**

TABLE 1: Optimized Distances (in Å) between the Li Interstitial and Neighboring Si Lattice Atoms for Both Positive and Negative Charge States[a]

	relaxed		unrelaxed
	Li^0/c-Si	Li^+/c-Si	Li/c-Si
Li−Si^{1st}	2.46	2.45	2.36
Li−Si^{2nd}	2.75	2.75	2.75
Si^{1st}-Si^{1st}	4.01	3.99	3.86

[a] For comparison, corresponding distances are also presented before the Si lattice relaxation. This clearly demonstrates an outward relaxation of the four Si first neighbors upon the Li insertion.

Figure 1. (Color online) Variation in the relative formation energy of Li^+ with respect Li^0 as a function of the Fermi level (ε_F) relative to the valence band maximum (E_V) for the computed Si gap of 0.62 eV.

of 5.457 Å; the effect of volume relaxation was also checked, and turns out to be unimportant as the 216-atom supercell is large enough to accommodate one or two Li atoms with no significant volume change (less than 1%). For geometry optimization and energy calculations, all atoms were fully relaxed using the conjugate gradient method until residual forces on constituent atoms become smaller than 5×10^{-2} eV/ Å; but the convergence criterion was tightened to 1×10^{-6} eV for vibrational frequency calculations. A $(2 \times 2 \times 2)$ k-point mesh in the scheme of Monkhorst-Pack was used for the Brillouin zone sampling.[30] Diffusion pathways and barriers were determined using the climbing-image nudged elastic band method with eight intermediate images for each hopping step.

3. Results and Discussion

3.1. Structure and Stability. First we determined the atomic structure and stability of interstitial Li in c-Si in the neutral (Li^0) and positive (Li^+) charge states. For both charge states, the tetrahedral (T) interstitial configuration (see the illustration above Table 1) is identified to be energetically the most favorable configuration. The Li insertion at the T site leads to a slight outward relaxation of the four Si first neighbors, i.e., 0.08 (0.07) Å displacement from their crystalline positions in the neutral (positive) case.

We examined other possible minimum-energy configurations for a Li interstitial. The hexagonal (H) state that is often another important local minimum for some interstitial atoms such as Si turns out to be a saddle point as detailed later. The ⟨110⟩-split state in which Li and Si atoms are aligned in the ⟨110⟩ direction while sharing a lattice site also appears to be unstable, while the ⟨110⟩-split dumbbell structure has been identified to be energetically most favorable for neutral Si and positively charged As−Si interstitial pair.[31] In addition, our calculation confirmed that the ⟨111⟩ bond-centered state in which Li is located between

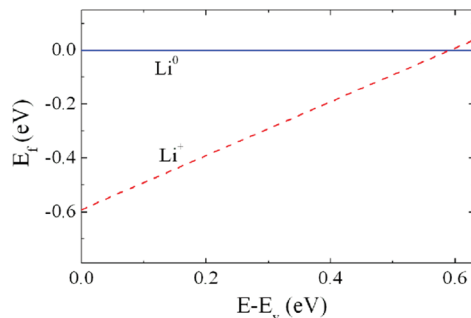two lattice Si atoms while the lattice Si atoms are substantially displaced outward in the ⟨111⟩ direction is highly unlikely.

Figure 1 shows the relative formation energy of Li^+ with respect to Li^0 at the T site, which is computed by $E_f^+ - E_f^0 = q(\varepsilon_F - \mu_i)$. The Fermi level ($\varepsilon_F$) is given relative to the valence band maximum (E_V). The ionization level (μ_i) is approximated by $E^+ + (E_v^+ + \mu_i) = E^0$, where E^+ and E^0 refer to the total energies of the positive and neutral states of the Li-containing supercell, and E_v^+ is the position of the valence band maximum in supercell E^+. In the periodic approach, a homogeneous background charge is included to maintain the overall charge neutrality of a charged supercell. Hence, to account for the electrostatic interaction with the background charge, a monopole correction was made to the total energy of the charged system.[32] For a point-like +1 charge in the 216-atom Si supercell, the monopole correction is approximated to be 0.11 eV. This approach seems to be reasonable considering the estimated charge state of Li^+ is +0.83 (*vide infra*), while the correction might be larger than the required adjustment if the charge on the impurity is significantly delocalized.

The predicted first donor (+/0) level is located near the conduction band minimum (E_c), i.e., $E_c - 0.02$ eV for the computed Si bandgap of 0.62 eV. The result suggests that Li interstitials might act like a shallow donor in c-Si. This is not surprising considering that Li has one valence electron ([He]$2s^1$) with a low electronegativity of 0.98, and can thereby be easily ionized via electron donation to the Si matrix (whose electronegativity is roughly scaled at 1.90). Our DFT-GGA calculations as a whole agree well with previous experiments[33] demonstrating that a Li atom introduced to c-Si remains at an interstitial site with T_d symmetry and behaves similarly to group-V shallow donors.

3.2. Bonding Mechanism. The amount of electron transfer from the inserted Li^0 to the Si matrix is estimated to be 0.83e from the grid-based Bader charge analysis,[34] special care was taken to ensure convergence with respect to the grid size. Likewise, in the positive charge system (Li^+), the Li charge state is also estimated to be +0.83. Analysis of the electronic density of states (DOS) for the Li^0/Si system [Figure 2(a)] shows a shift of the Fermi level above the conduction band minimum of Si (while there is no noticeable change in the Li^+/Si case [Figure 2(b)]). This indicates that the transferred charge from Li^0 partially fills the antibonding sp^3 state of neighboring Si atoms, which in turn weakens corresponding Si−Si bonds. The results clearly support that the Si network can be destabilized by lithiation, leading to the formation of various Si−Li alloy phases as also evidenced by earlier experiments.[19−22]

We analyzed the bonding mechanism for Li^0 in the T configuration by calculating charge density differences before

17944 *J. Phys. Chem. C, Vol. 114, No. 41, 2010*
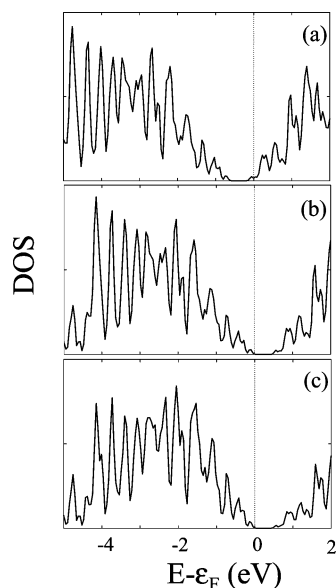
Kim et al.

Figure 2. Electronic density of states (DOS) for the host Si matrix with (a) Li[0], (b) Li^{+}, and (c) no Li. The vertical dotted line indicates the Fermi level (ε_F) position.
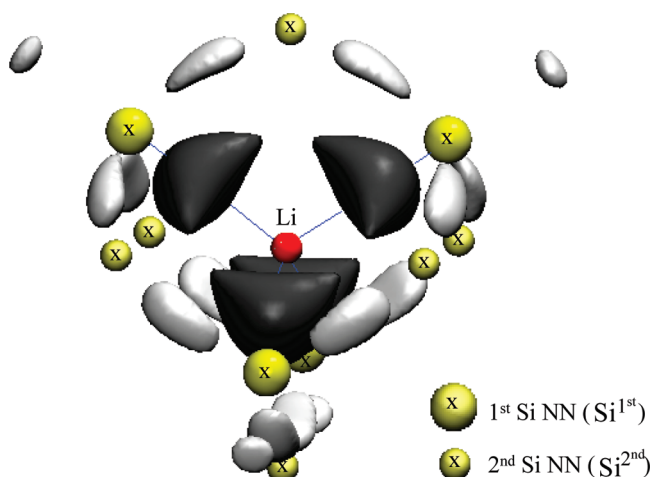

Figure 3. (Color online) Valence charge density difference plot for Li[0] insertion. The charge density difference ($\Delta\rho$) is calculated by subtracting the charge densities of an isolated Li[0] and the Si matrix (with no Li[0]) from the total charge density of the Li[0]/Si matrix with no atomic displacement, i.e., $\Delta\rho = \rho(\text{Li}^0/\text{Si}) - \rho(\text{Li}^0) - \rho(\text{Si})$. The positions of the Li, and its first and second Si nearest neighbors (NN) are indicated. The dark gray and light gray isosurfaces represent the regions of charge gain ($+0.019$ e/Å^3) and loss (-0.012 e/Å^3), respectively.

and after the Li insertion. As presented in Figure 3, our calculation demonstrates charge accumulation in the region between the Li and each of its four nearest Si neighbors with a noticeable shift toward the Si atom. This suggests that the Si−Li bond can be characterized by polar covalent. Another important feature is that electron densities are noticeably depleted in the nearby Si−Si covalent bonding regions, especially between the first and second nearest Si atoms. The charge depletion in the middle region between two Si−Si atoms is indicative of a weakening of its covalent bond, as also demonstrated by the aforementioned LDOS analysis. In addition, the charge density difference plot in Figure 3 shows that the charge transferred from the Li[0] is largely localized within the first nearest Si lattice atoms, which in turn effectively screens the positively ionized Li interstitial.
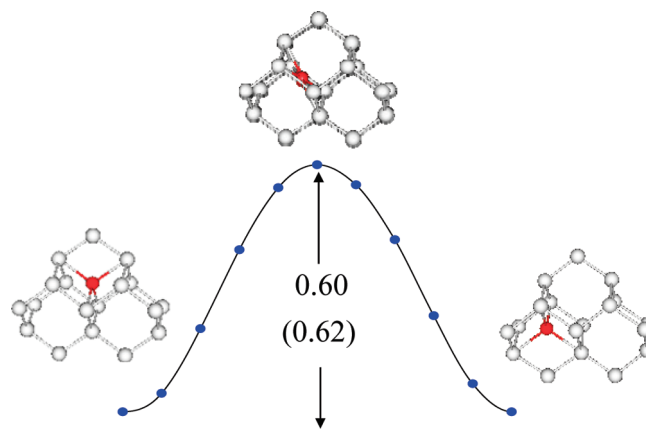

Figure 4. (Color online) Predicted diffusion path for Li in *c*-Si. The energy variation is given in eV; the diffusion barriers for Li[0] and Li^{+} are predicted to be 0.60 and 0.62 eV, respectively. The black (red) and light gray balls represent Li and Si atoms.

3.3. Diffusion. As illustrated in Figure 4, a Li interstitial may undergo migration by jumping between adjacent T sites via the H site which turns out to be a saddle point. The transition H state is predicted to be 0.60 (0.62) eV above the local-minimum T state in the neutral (positive) charge state, which is close to 0.58 eV for Li^{+} from previous calculations.[35]

We evaluated the temperature-dependent diffusion coefficients of Li[0]/Li^{+} using the Arrhenius equation, $D = D_0 \exp(-E_a/k_B T)$, where E_a refers to the activation barrier for diffusion, k_B is the Boltzmann constant, and T is the temperature. Within harmonic transition state theory, the prefactor (D_0) can be derived by $D_0 = (1/2\alpha) \lambda l^2 v_0$, where α is the dimensionality of the diffusion space (which is 3 in the three-dimensional system considered), λ is the number of equivalent diffusion paths, l is the jump length between two adjacent local minima, and v_0 is the attempt frequency.[36,37] For the T → H → T diffusion event, there are four equivalent routes with a jump length of 2.36 Å. Using the Vineyard equation,[36] we can estimate the attempt frequency v_0 by the following:

$$v_0 = \prod_{i=1}^{3N} v_i^* \bigg/ \prod_{i=1}^{3N-1} v_i^{**}$$

where v_i^* and v_i^{**} are the harmonic vibrational frequencies at the minimum and saddle points, respectively. The vibrational frequencies were determined by diagonalizing a Hessian matrix obtained from numerical differentiation of forces that were calculated by displacing 28 nonfrozen atoms surrounding the diffusing Li in the $\pm x$, $\pm y$, and $\pm z$ directions by 0.02 Å. At the saddle point, there was one imaginary frequency at around 307i cm^{-1} for Li[0] (312i cm^{-1} for Li[1+]). As summarized in Table 2, v_0 and D_0 for Li^{+} diffusion are estimated to be 8.57 THz and 3.18×10^{-3} cm^2/sec, in good agreement with $v_0 = 10.11$ THz and $D_0 = 3.72 \times 10^{-3}$ cm^2/sec from previous calculations.[35] For the Li[0] case, v_0 and D_0 values are estimated to be 8.59 THz and 3.19×10^{-3} cm^2/sec, close to the Li^{+} case. Taking the prefactors and activation barriers, Li diffusion coefficients are estimated to be $D = 1.04 \times 10^{-13}$ cm^2/sec and 2.27×10^{-13} cm^2/sec at 298 K in the positive and neutral charge states, respectively. The predicted diffusivities are close to previous theoretical results (e.g., 5.78×10^{-13} cm^2/sec for Li^{+})[35] and also within the range of experimental values reported in the literature (2×10^{-14} cm^2/sec[38]).

Nature and Behavior of Li Atoms in Si

J. Phys. Chem. C, Vol. 114, No. 41, 2010 **17945**

TABLE 2: Predicted Values of the Attempt Frequency (v_0) and Activation Energy (E_a) for Li Diffusion[a]

		v_0 (THz)	E_a (eV)	D_0 (10^{-3} cm²/sec)	D (at 298 K) (10^{-13} cm²/sec)
this work	Li^0	8.59	0.60	3.19	2.27
	Li^+	8.57	0.62	3.18	1.04
cal[b]	Li^+	10.11	0.58	3.72	5.78
exp[c]	Li^+		0.57–0.79	1.9–9.4	~17.9

[a] Here, the prefactor (D_0) and diffusivity (D) are estimated by the following: $D_0 = (1/2\alpha)\,\lambda l^2\,v_0$ where α is the dimensionality of the diffusion space (which is 3 in the three-dimensional system considered), λ is the number of equivalent diffusion paths, and l is the jump length between two adjacent minima; and $D = D_0 \exp(-E_a/k_B T)$, where k_B is the Boltzmann constant and T is the temperature. Previous calculation and experimental values available in the literature are also presented for comparison. [b] Ref 35. [c] Ref 38.
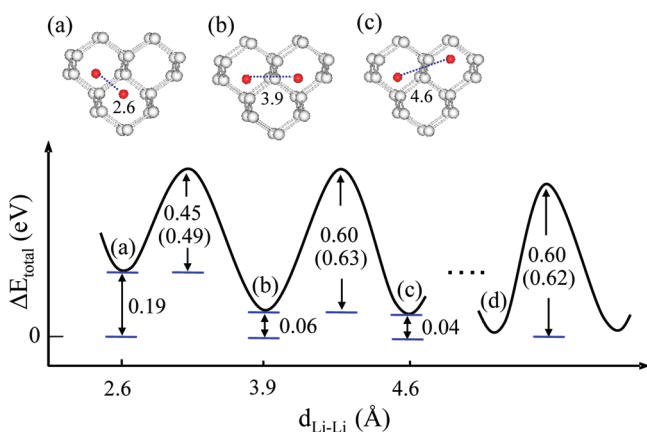

Figure 5. (Color online) Variation in the total energy as a function of the distance between two Li^0 interstitials with respect to the fully separated state [(d)]. The black (red) and light gray balls represent Li and Si atoms. For comparison, diffusion barriers for the Li^+–Li^+ case are also presented in parentheses.

3.4. Li–Li Interaction. Finally, we looked at the interaction between two Li^0 interstitials in *c*-Si. Figure 5 shows the variation in the relative energies with respect to the fully separated state [(d)] for various Li–Li distances; one Li was at a T site and the other was placed at the first [(a)], second [(b)], or third [(c)] nearest T site. The relative energies for (a), (b), and (c) are 0.19, 0.06, and 0.04 eV higher compared to (d). The total energy increase with decreasing the Li–Li distance is apparently caused by the repulsive interaction between the positively ionized Li interstitials; however, the force of repulsion tends to rapidly diminish as a result of effective screening as discussed earlier. Owing to the repulsive interaction, the diffusion barrier for (a) → (b) is lowered to 0.45 eV, as opposed to 0.6 eV for the noninteracting case. This finding also implies that Li interstitials favorably remain isolated, rather than clustered, at sufficiently low concentrations. For comparison, we also looked at the Li^+–Li^+ interaction; the result looks similar to the Li^0–Li^0 case, as presented in Figure 5.

Our calculations also show that the Li–Li distances are 2.59, 3.91, and 4.58 Å, respectively, for the (a), (b), and (c) cases, which are larger than 2.36, 3.86, and 4.52 Å for corresponding first, second, and third nearest T sites in *c*-Si (with no Li interstitial). This is not surprising considering the volume expansion of the Si structure upon Li introduction. The results clearly demonstrate that lithiation will rather easily lead to destabilization of the host Si network and subsequent formation of new Si–Li alloy phases, accompanied with significant volume expansion.

4. Conclusions

Using DFT-GGA calculations, we examined the structure, stability, diffusion, and bonding mechanism of a single Li interstitial atom in *c*-Si in the neutral and positive charge states. We also looked at the interaction between two Li interstitials and the effect of Li incorporation on the stability of the Si lattice. For both Li^0 and Li^+, the tetrahedral (T) state turns out to be energetically most favored. The first donor (+/0) level is predicted to be at $E_c - 0.02$ eV for the computed Si bandgap of 0.62 eV, suggesting that interstitial Li would act as an effective donor in *c*-Si. Our DFT calculation shows that interstitial Li may undergo diffusion with a moderate barrier of ~0.6 eV. Taking the computed prefactor of ~3 × 10^{-3} cm²/sec, the Li diffusion coefficient is estimated to be on the order of 10^{-13} cm²/sec at room temperature, while there is no significant difference between Li^0 and Li^+. We find that the interaction between Li^0 interstitials is repulsive due to their positive ionization; the placement of two Li^0 atoms at adjacent T sites is 0.19 eV less favorable compared to when they are fully separated. This implies that Li interstitials favorably remain isolated, rather than clustered. The incorporation of Li^0 at the T site results in noticeable outward displacement of the four Si first neighbors by 0.08 Å from their crystalline positions. Our calculation also shows that the charge transferred from Li^0 is largely localized within the first nearest Si lattice atoms, which in turn effectively screens the positively ionized Li interstitial. Our analysis of electronic density of states (DOS) highlights that the electron transfer leads to partial filling of the antibonding sp^3 states of neighboring Si atoms, which in turn weakens corresponding Si–Si bonds. This also clearly indicates that the host Si lattice can be easily destabilized by Li insertion. The fundamental findings assist in understanding the dynamic behavior of Li atoms and the nature of their interaction with the host Si matrix, particularly during the early stages of lithiation.

References and Notes

(1) Winter, M.; Besenhard, J. O. Electrochemical Lithiation of Tin and Tin-Based Intermetallics and Composites. *Electrochim. Acta* **1999**, *45*, 31.

(2) Sharma, R. A.; Seefurth, R. N. Thermodynamic Properties of the Lithium-Silicon System. *J. Electrochem. Soc.* **1976**, *123*, 1763.

(3) Boukamp, B. A.; Lesh, G. C.; Huggins, R. A. All-Solid Lithium Electrodes with Mixed-Conductor Matrix. *J. Electrochem. Soc.* **1981**, *128*, 725.

(4) Beaulieu, L. Y.; Eberman, K. W.; Turner, R. L.; Krause, L. J.; Dahn, J. R. Colossal Reversible Volume Changes in Lithium Alloys. *Electrochem. Solid-State Lett.* **2001**, *4*, A137.

(5) Ryu, J. H.; Kim, J. W.; Sung, Y. E.; Oh, S. M. Failure Modes of Silicon Powder Negative Electrode in Lithium Secondary Batteries. *Electrochem. Solid-State Lett.* **2004**, *7*, A306.

(6) Obrovac, M. N.; Christensen, L. Structural Changes in Silicon Anodes during Lithium Insertion/Extraction. *Electrochem. Solid-State Lett.* **2004**, *7*, A93.

(7) Maranchi, J. P.; Hepp, A. F.; Kumta, P. N. High Capacity, Reversible Silicon Thin-Film Anodes for Lithium-Ion Batteries. *Electrochem. Solid-State Lett.* **2003**, *6*, A198.

(8) Netz, A.; Huggins, R. A.; Weppner, W. The Formation and Properties of Amorphous Silicon As Negative Electrode Reactant in Lithium Systems. *J. Power Sources* **2003**, *119–121*, 95.

(9) Bourderau, S.; Brousse, T.; Schleich, D. M. Amorphous Silicon As a Possible Anode Material for Li-Ion Batteries. *J. Power Sources* **1999**, *81–82*, 233.

(10) Hatchard, T. D.; Dahn, J. R. *In Situ* XRD and Electrochemical Study of the Reaction of Lithium with Amorphous Silicon. *J. Electrochem. Soc.* **2004**, *151*, A838.

(11) Gao, B.; Sinha, S.; Fleming, L.; Zhou, O. Alloy Formation in Nanostructured Silicon. *Adv. Mater.* **2001**, *13*, 816.

(12) Graetz, J.; Ahn, C. C.; Yazami, R.; Fultz, B. Highly Reversible Lithium Storage in Nanostructured Silicon. *Electrochem. Solid-State Lett.* **2003**, *6*, A194.

(13) Chan, C. K.; Peng, H.; Liu, G.; McIlwrath, K.; Zhang, X. F.; Huggins, R. A.; Cui, Y. High-Performance Lithium Battery Anodes Using Silicon Nanowires. *Nat. Nanotechnol.* **2008**, *3*, 31.

(14) Beaulieu, L. Y.; Hewitt, K. C.; Turner, R. L.; Bonakdarpour, A.; Abdo, A. A.; Christensen, L.; Eberman, K. W.; Krause, L. J.; Dahn, J. R. The Electrochemical Reaction of Li with Amorphous Si−Sn Alloys. *J. Electrochem. Soc.* **2003**, *150*, A149.

(15) Mao, O.; Turner, R. L.; Courtney, I. A.; Fredericksen, B. D.; Buckett, M. I.; Krause, L. J.; Dahn, J. R. Active/Inactive Nanocomposites as Anodes for Li-Ion Batteries. *Electrochem. Solid-State Lett.* **1999**, *2*, 3.

(16) Fleischauer, M. D.; Topple, J. M.; Dahn, J. R. Combinatorial Investigations of Si−M (M = Cr + Ni, Fe, Mn) Thin Film Negative Electrode Materials. *Electrochem. Solid-State Lett.* **2005**, *8*, A137.

(17) Beaulieu, L. Y.; Hatchard, T. D.; Bonakdarpour, A.; Fleischauer, M. D.; Dahn, J. R. Reaction of Li with Alloy Thin Films Studied by *In Situ* AFM. *J. Electrochem. Soc.* **2003**, *150*, A1457.

(18) (a) Nazri, G. A.; Pistoia, G. *Lithium Batteries Science and Technology*; Kluwer Academic, Plenum: Boston, 2004. (b) Anani, A.; Crouch-Baker, S.; Huggins, R. A. Kinetic and Thermodynamic Parameters of Several Binary Lithium Alloy Negative Electrode Materials at Ambient Temperature. *J. Electrochem. Soc.* **1987**, *134*, 3098.

(19) Anantharaman, T. R. *Metallic Glasses: Production Properties and Applications*; Trans Tech Publications: Uetikon-Zurich, 1984.

(20) Massalski, T. B.; Okamoto, H.; *Binary Alloys Phase Diagrams*; ASM International, Materials Park, OH, 1990.

(21) Stearns, L. A.; Gryko, J.; Diefenbacher, J.; Ramachandran, G. K.; McMillan, P. F. Lithium Monosilicide (LiSi), a Low-Dimensional Silicon-Based Material Prepared by High Pressure Synthesis: NMR and Vibrational Spectroscopy and Electrical Properties Characterization. *J. Solid State Chem.* **2003**, *173*, 251.

(22) Kubota, Y.; Escano, M. C. S.; Nakanishi, H.; Kasai, H. Crystal and Electronic Structure of $Li_{15}Si_4$. *J. Appl. Phys.* **2007**, *102*, 053704.

(23) Kubota, Y.; Escano, M. C. S.; Nakanishi, H.; Kasai, H. Electronic Structure of LiSi. *J. Alloys Compd.* **2008**, *458*, 151.

(24) van Leuken, H.; de Wijs, G. A.; van der Lugt, W.; de Groot, R. A. Electronic Structure of $Li_{12}Si_7$. *Phys. Rev. B* **1996**, *53*, 10599.

(25) Limthongkul, P.; Jang, Y. I.; Dudney, N. J.; Chiang, Y. M. Electrochemically-Driven Solid-State Amorphization in Lithium-Silicon Alloys and Implications for Lithium Storage. *Acta. Mater.* **2003**, *51*, 1103.

(26) Blochl, P. E. Projector Augmented-Wave Method. *Phys. Rev. B* **1994**, *50*, 17953.

(27) Kresse, G.; Hafner, J. Ab Initio Molecular Dynamics for Liquid Metals. *Phys. Rev. B* **1993**, *47*, 558.

(28) Kresse, G.; Furthmuller, J. Efficiency of Ab-Initio Total Energy Calculations for Metals and Semiconductors Using a Plane-Wave Basis Set. *Comput. Mater. Sci.* **1996**, *6*, 15.

(29) Kresse, G.; Furthmuller, J. Efficient Iterative Schemes for Ab Initio Total-Energy Calculations Using a Plane-Wave Basis Set. *Phys. Rev. B* **1996**, *54*, 11169.

(30) Monkhorst, H. J.; Pack, J. D. Special Points for Brillouin-Zone Integrations. *Phys. Rev. B* **1976**, *13*, 5188.

(31) Harrison, S. A.; Edgar, T. F.; Hwang, G. S. Interstitial-Mediated Mechanisms of As and P Diffusion in Si: Gradient-Corrected Density-Functional Calculations. *Phys. Rev. B* **2006**, *74*, 195202.

(32) Makov, G.; Payne, M. C. Periodic Boundary Conditions in Ab Initio Calculations. *Phys. Rev. B* **1995**, *51*, 4014.

(33) Aggarwal, R. L.; Fisher, P.; Mourzine, V.; Ramdas, A. K. Excitation Spectra of Lithium Donors in Silicon and Germanium. *Phys. Rev.* **1965**, *138*, A882.

(34) Henkelman, G.; Arnaldsson, A.; Jonsson, H. A fast and Robust Algorithm for Bader Decomposition of Charge Density. *Comput. Mater. Sci.* **2006**, *36*, 354.

(35) Milman, V.; Payne, M. C.; Heine, V.; Needs, R. J.; Lin, J. S.; Lee, M. H. Free Energy and Entropy of Diffusion by Ab Initio Molecular Dynamics: Alkali Ions in Silicon. *Phys. Rev. Lett.* **1993**, *70*, 2928.

(36) Weiser, K. Theory of Diffusion and Equilibrium Position of Interstitial Impurities in the Diamond Lattice. *Phys. Rev.* **1962**, *126*, 1427.

(37) Harding, J. H. Computer Simulation of Defects in Ionic Solids. *Rep. Prog. Phys.* **1990**, *53*, 1403.

(38) Canham, L. T. *Properties of Silicon, Electronic Materials Information Service (EMIS)*, Ravi, K. V., Hecking, N., Fengwei, W., Xiangqin, Z., Alexsandrev, L. N., Eds.; London, Dataviews Series No. 4, INSPEC, 1988.